

The role of cells refractory to productive infection in acute hepatitis B virus infection dynamics-Supplementary Material

September 26, 2006

Stanca M. Ciupe, Ruy M. Ribeiro, Patrick W. Nelson, Alan S. Perelson

We have organized the supplementary material into two parts. In the first section we provide more details on the algorithms we use to fit the unknown parameters in our models. In the second section we present numerical results for the alternative models described in the paper. We explain the differences between these models and the information that we can extract from them.

1 Parameter fitting

As mentioned in the Methods section of the main paper, to estimate the initial guesses for the parameter estimation for model (1) in the text, we used a hill climbing Monte Carlo algorithm. For that we define an objective function

$$J(x) = \sqrt{\sum_{i=1}^n (\log(V(t_i, x)) - \log(\bar{V}(t_i)))^2}$$

where n is the number of data points available, $x = [\alpha, \mu, \mu_1, \tau, \rho, p, k]^T$ is the vector of parameters to be determined, $V(x, t_i)$ is the viral load, at time t_i and parameters x , predicted by our model and $\bar{V}(t_i)$ represents the data value at time t_i . For each set of parameters, a numerical solution of the initial value problem, $V(t_i, x)$, is generated via a modification of the Euler algorithm, designed to handle the delays of the model [1]. The parameter set that best fits the data occurs when $J(x)$ is minimized over the parameter region.

Initially we choose the parameters randomly from a uniform distribution on a predetermined interval. We first iterated the Monte Carlo algorithm 12,000 times with the following parameter ranges $\mu \in (0, 1)$, $\mu_1 \in (0, 1)$, $\alpha \in (0, 10^{-3})$, $\tau \in (0, 50)$, $\rho \in (0, 0.5)$, $p \in (0, 500)$ and $k \in (0, 10^{-9})$. From this process we select the set of parameters for the current "best model", *i.e.*, that with smallest $J(x)$. We then repeat the procedure (8,000 more iterations), but the parameters are selected from a range around the current "best model". That is, for a given parameter, x , the algorithm will look locally in a window between $x - a \times x$ and $x + a \times x$, where a has an initial value of 0.01. By varying the size of this "window", *i.e.* the a value, we can both search the parameter space and local

regions to minimize $J(x)$, by making very small changes in the parameters. This algorithm also has the advantage of avoiding stagnation in local maxima, because one can increase the window width to find fits better than the local minimum of $J(x)$.

Once we found the vector of parameters

$$\hat{x} = (\hat{\alpha}, \hat{\mu}, \hat{\mu}_1, \hat{\tau}, \hat{\rho}, \hat{p}, \hat{k})$$

that minimizes the functional J , we used these values as the initial guesses in a standard Levenberg-Marquardt search algorithm.

We then calculated 95% confidence intervals for these estimates by bootstrapping the fit residuals. Briefly, for each patient, let $\hat{\Upsilon} = \{\hat{\epsilon}_1, \hat{\epsilon}_2, \dots, \hat{\epsilon}_n\}$ be the set of residuals defined by

$$\hat{\epsilon}_i = \bar{V}(t_i) - V(t_i, \hat{x}(t_i)), \quad (1.1)$$

for all data time points t_i , with $i \in \{1, 2, \dots, n\}$. Next, we define $\Upsilon^* = \{\epsilon_1^*, \epsilon_2^*, \dots, \epsilon_n^*\}$, where, for each i , ϵ_i^* are values drawn at random with replacement from the set $\hat{\Upsilon}$. We form the sets $V_j^* = \{V_{j1}^*, V_{j2}^*, \dots, V_{jn}^*\}$ of independent and identically distributed pseudo-observations, where

$$V_{ji}^* = V(t_i, \hat{x}(t_i)) + \epsilon_i^*. \quad (1.2)$$

Numerically we generate 200 bootstrap samples $V_1^*, V_2^*, \dots, V_{199}^*$, and for each of them we used the Levenberg-Marquardt algorithm above to calculate the correspondent vector of parameters. From these, we directly calculate the 95% quantile confidence interval for each parameter estimate.

For the alternative models shown below, we calculated a set of parameters consistent with the data using the Monte Carlo algorithm described.

2 Alternative models

In order to better understand the predictions provided by the model we examined the sensitivity of our results to some of the basic assumptions of the model. We are mainly interested in two issues: the role of the refractory cell population and the nature of both the cytolytic and non-cytolytic immune responses.

In the first alternative model, we remove the R population, and assume that the noncytolytic immune response causes infected cells to return to uninfected cells, (*i.e.*, T_1^* goes to T at rate ρ). The results of fitting this model to the data are shown in Fig. S1. As uninfected cells arise the virus resurges giving rise to the prediction of multiple viral peaks, which are not seen in the data.

In the second alternative model we remove the non-cytolytic effect (*i.e.*, $\rho = 0$). There is no recovered population as we assume recovery is cytokine dependent. To compensate for the generation of uninfected hepatocytes, the best-fit model predicts a large amount of killing of infected cells, resulting in substantial decreases in total cell numbers. This model is also unable to fit the viral load data, which starts increasing at the end of the first phase of decline, due to generation of through proliferation of new uninfected cells (see Fig. S2). This version of the model predicts unrealistic reductions in liver size, of up to 90% (Figures S2) since cytolytic responses are the main mechanism

of viral clearance.

To analyze the immune response in more detail, we built three additional models. In the third alternative model, we removed the cytolytic immune response, by setting μ and μ_1 to zero (Figure S3). This model, with two fewer parameters than the original model, was remarkably consistent with the data. Indeed, comparisons based on the F-test demonstrate that this model is statistically equivalent to model (1) in the main text for all patients ($P > 0.57$). Given model S3 consistency with the data, we also explored a model with just a non-cytolytic response, but independent from the effector cell dynamics. That is, the term in model (1) ρET_1^* becomes ρT_1^* in model S4. We show these fits in Figure S4. This model generates a monophasic decay in viral load (Figure S4). Further, for patients p1 and p4 the model does not fit the peak viral load nearly as well as model (1) in the main text. However, when we take into account that this model has only 5 parameters, instead of 8, there is no statistically significant improvement in the sum of squared residuals in model (1) compared to this simpler model by an F-test ($P > 0.27$).

In another alternative model, we consider the effect of removing both the cytolytic and non-cytolytic effects by setting E to be zero. This is meant to mimic experiments in which anti-CD8 monoclonal antibodies were used to remove the CD8⁺ T cells responsible for the cytolytic and non-cytolytic immune responses in HBV infected chimpanzees [2]. The results show that the viral load reaches a set point at the peak of the infection and the clearance does not occur (Figure S5). This is similar to the experimental results in CD8-depleted chimpanzees [2].

In the last alternative model we consider two populations of productively infected hepatocytes (T_1^* , T_2^* , with single or multiple cccDNA nuclear copies, respectively). Both types of infected cells can be killed by the immune response at rate μE per cell. Both classes of infected cells proliferate in a manner similar to the uninfected cells. However, since cccDNA does not replicate upon cell division, when a T_1^* cell divides, it will produce one infected cell with one copy of cccDNA, keeping T_1^* unchanged, and one cell with no cccDNA [3], which we put into the T population. Division of infected cells occurs at a growth rate r . Finally, T_1^* can also be lost due to synthesis of new cccDNA and transition into the T_2^* class at rate z . The results are similar with the ones in model (1) (Fig. S7). Although we consider this model to be more biological, the results show no statistically significant improvement in the sum of squared residuals in this model compared to model (1) by an F-test ($P > 0.92$).

References

- [1] Ciupe, S.M., deBivort, B., Bortz, D.M., & Nelson, P.W. (2006) *Math. Biosci.* **200**, 1–27.
- [2] Thimme, R., Wieland, S., Steiger, C., Ghayeb, J., Reimann, K.A., Purcell, R.H., & Chisari, F.V. (2003) *J. Virol.* **77**, 68–76.
- [3] Zhang, Y-Y, Zhang, B-H, Theele, D, Litwin, S, Toll, E, & Summers, J (2003) *Proc. Natl. Acad. Sci. USA* **100**, 12372–12377.

Figure S1. Results of fitting an alternative model with no R population to the HBV DNA data. The best fit of the model (red dashed line) to patient data (*), and hepatocytes loss as a percentage of T_{max} (green solid line).

Figure S2. Results of fitting an alternative model with no noncytolytic effect to the HBV DNA data. The best fit of the model (red dashed line) to patient data (*) and hepatocytes loss as a percentage of T_{max} (green solid line).

Figure S3 Results of fitting an alternative model with $\mu = \mu_1 = 0$ to the data. The best fit of the model (red dashed line) to patient data (*).

Figure S4 Results of fitting an alternative model with $\mu = \mu_1 = \alpha = 0$ to the data. The best fit of the model (red dashed line) to patient data (*).

Figure S5 Results of fitting an alternative model with no E population to the data. The best fit of the model (red dashed line) to patient data (*).

Figure S6 The predicted temporal relationship of the cytolytic response to the level of infection and the ALT. Displayed for each patient are the cytolytic immune response, $\mu T_1^*(t)E(t) + \mu T_2^*(t)E(t) + \mu_1 R(t)E(t)$ (green line) and ALT (o).

Figure S7. Results of fitting the model with two classes of infected cells to each patient's HBV DNA data and the relationship between effector cells and serum ALT during the acute phase of the infection. The best fit of the model (dashed line) to HBV DNA patient data (*). The measured serum ALT (o), which was not used in data fitting, compares well with the predicted dynamics of the HBV-specific effector cell response (solid line).

Figure S1

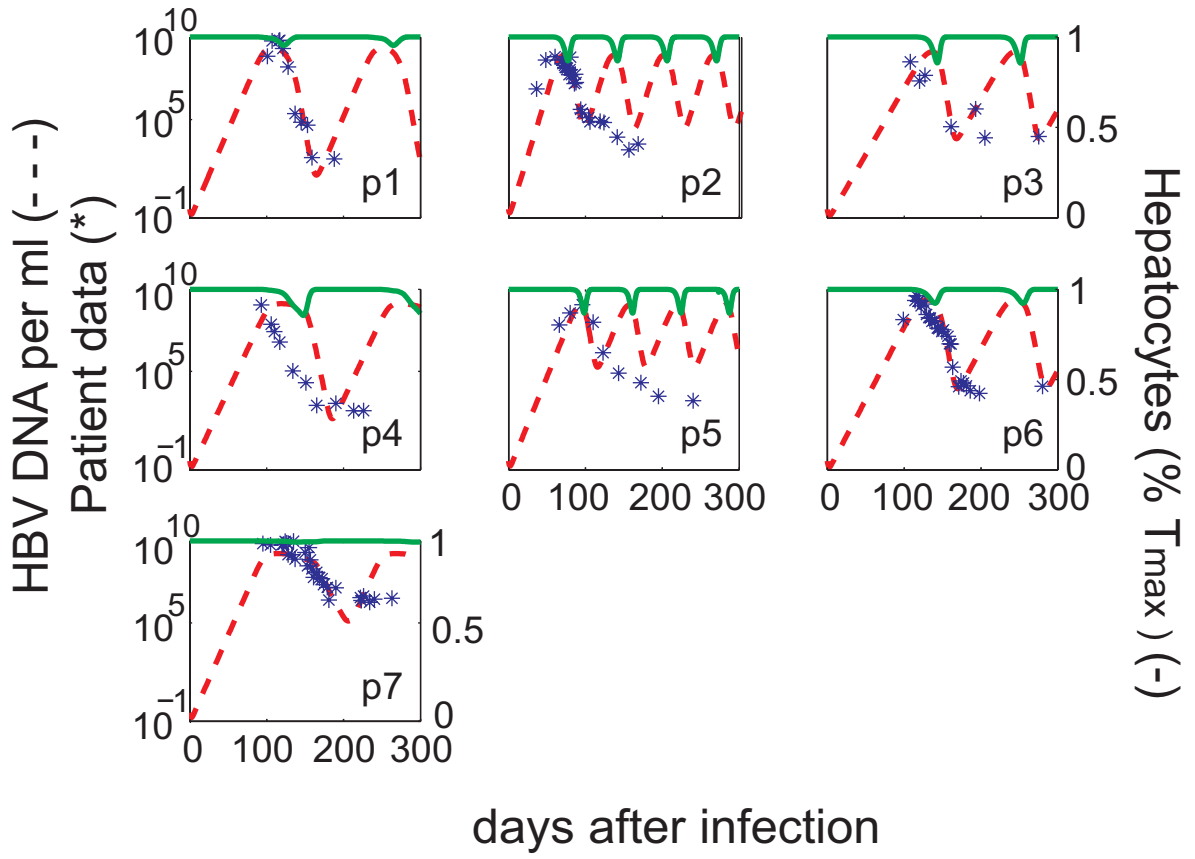


Figure S2

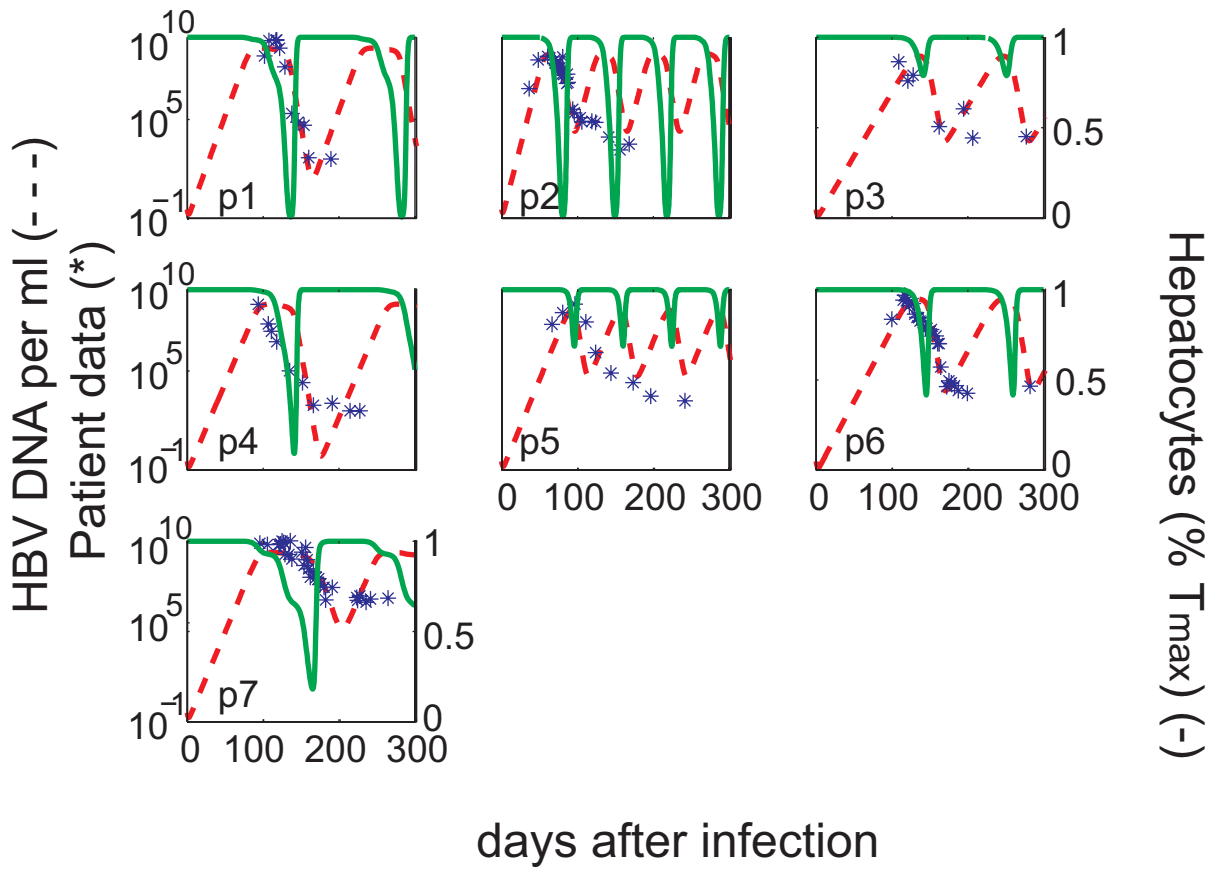


Figure S3

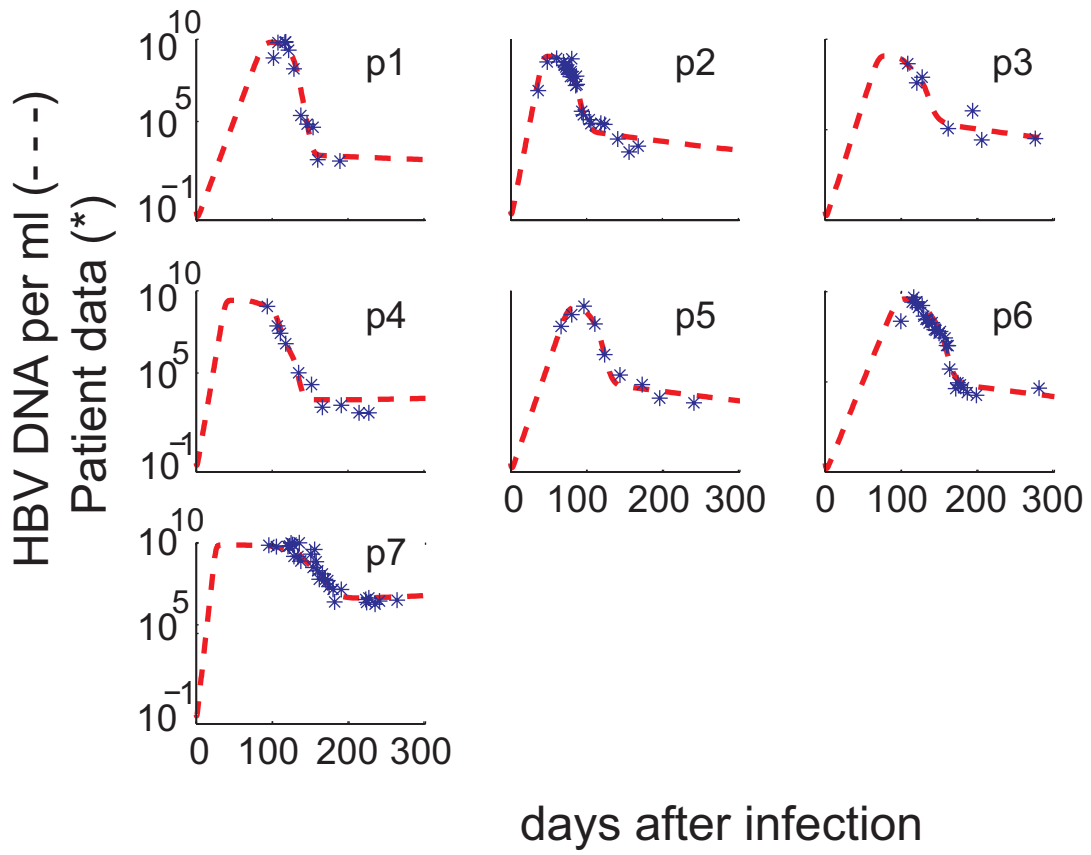


Figure S4

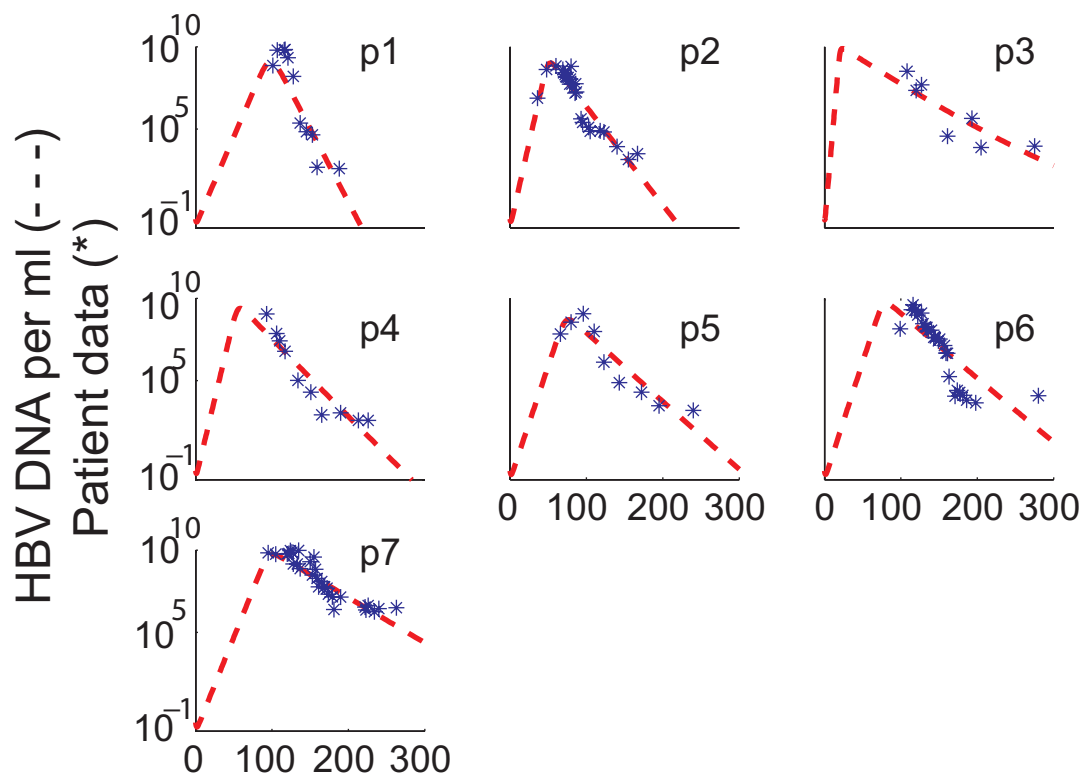


Figure S5

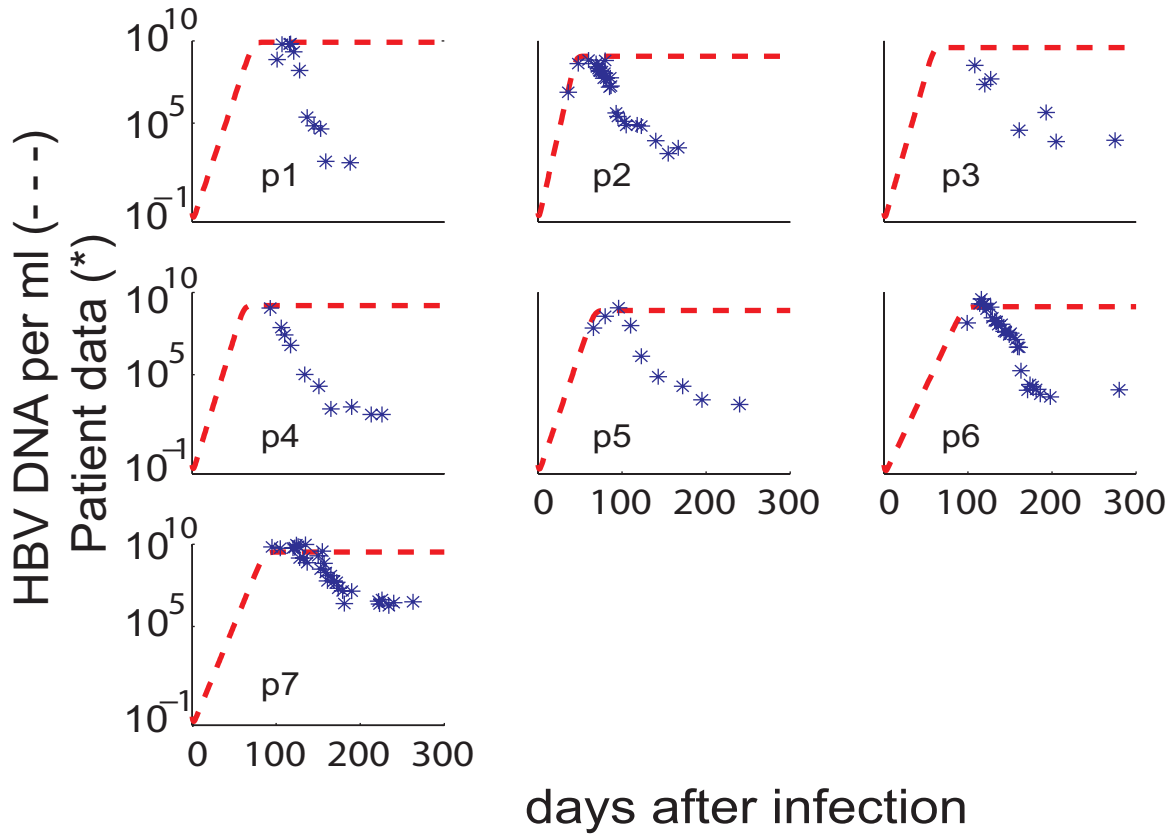


Figure S6

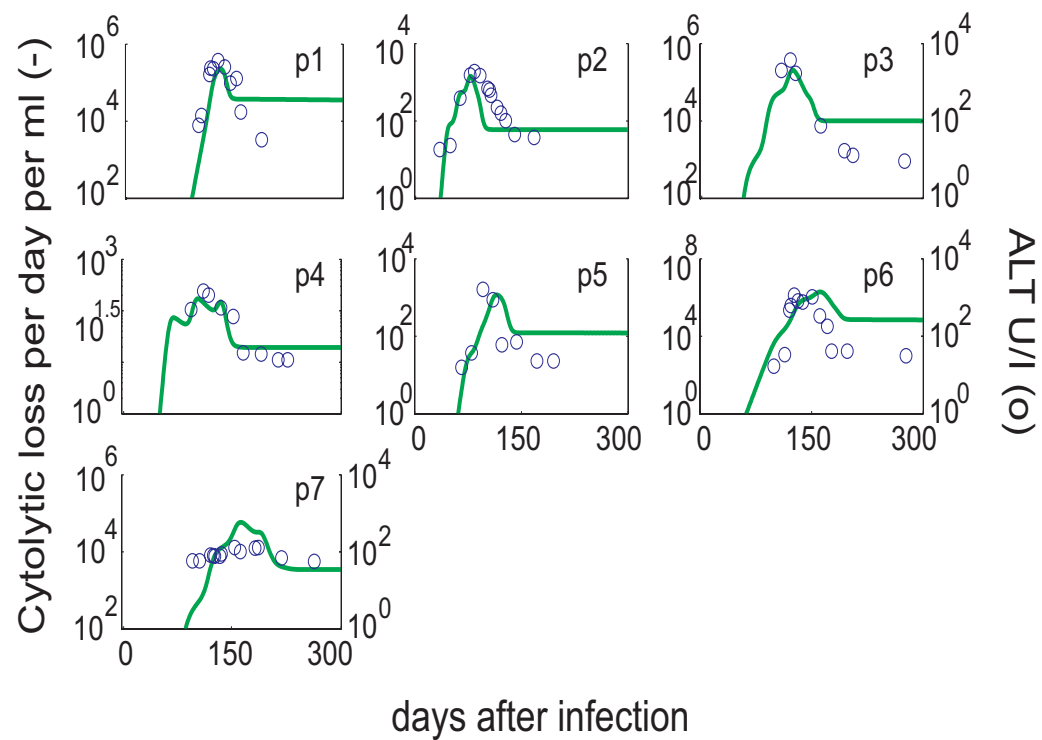


Figure S7

